Available online at www.sciencedirect.com
ScienceDirect
Journal of Organometallic Chemistry 692 (2007) 2324–2333
Journal of Organometallic Chemistry
www.elsevier.com/locate/jorganchem

Synthesis, electrochemistry, and photophysical properties of binuclear ruthenium(II)–terpyridine complexes comprising redox-active ferrocenyl spacer

Teng-Yuan Dong *, Mei-Ching Lin, Shu-Wei Chang, Chih-Chien Ho, Shu-Fan Lin, Liangshiu Lee

Department of Chemistry, Center for Nanoscience and Nanotechnology, National Sun Yat-Sen University, Kaohsiung, Taiwan

Received 4 January 2007; received in revised form 5 February 2007; accepted 9 February 2007
Available online 20 February 2007

Abstract

In attempting to perturb the electronic properties of the spacer, we now describe an interesting example of Ru^{2+}–tpy (tpy = terpyridine) complexes with 1,1′-bis(ethynyl)polyferrocenyl moiety attached directly to the 4′-position of the tpy ligand (tpy–C≡C–$(fc)_n$–C≡C–tpy; fc = ferrocenyl; $n = 2$–3). Complexes of Ru^{2+}–tpy have room-temperature luminescence in H_2O/CH_3CN (4/1) solution. The ground-state HOMO and LUMO energies were probed by electrochemical measurements and the excited-state photophysical properties were probed by UV–Vis absorption spectroscopy and luminescence spectroscopy. The redox behavior of $[(tpy)Ru^{II}$–tpy–C≡C–$(fc)_n$–C≡C–tpy–$Ru^{II}(tpy)]^{4+}$ complex is dominated by the Ru^{2+}/Ru^{3+} redox couple ($E_{1/2}$ from 1.35 to 1.39 V), Fe^{2+}/Fe^{3+} redox couples ($E_{1/2}$ from 0.4 to 1.0 V) and $tpy/tpy^{-}/tpy^{2-}$ redox couples ($E_{1/2}$ from −1.3 to −1.5 V). Electrochemical data, UV absorption and emission spectra indicate that the π-delocalization in the spacer is enhanced by the insertion of ethynyl unit. Interestingly, the insertion of ethynyl unit into the main chain causes a dramatic increase of phosphorescence yield (1.48×10^{-4} for $n = 2$; 1.13×10^{-4} for $n = 3$), triplet lifetime (67 ns for $n = 2$; 24 ns for $n = 3$), and emission intensity. The biferrocenyl spacer can be converted into mixed-valence biferrocenium spacer, which gives a more effective π-delocalization along main chain, by selective chemical oxidation of ferrocenyl unit. In deoxygenated H_2O/CH_3CN (4/1) solution at 25 °C, the oxidized complex of $[(tpy)Ru^{II}$–tpy–C≡C–$(fc)_2$–C≡C–tpy–$Ru^{II}(tpy)]^{5+}$ is nonemissive. The presence of lower energy ferrocenium-centered $[Ru_a^{II}$–tpy^{-}–fc^{III}–fc^{III}–tpy–$Ru_b^{II}]$excited-state provides an additional channel for excited-state decay. The mixed-valence biferrocenium center acts as an efficient quencher for the MLCT excited-state.

Keywords: Molecular wire; Time-resolved spectroscopy; Luminescence; Electrochemistry; Metallocene

1. Introduction

Over the past decade, complexes containing unsaturated form of organic linear spacers end-capped by various transition metal centers have been proposed as models for molecular wires. In this context, end-capping of unsaturated organic spacers with redox-active groups, such as ruthenium(II) polypyridine metal centers, have been most studied where they are intended to promote long-range electron or energy transfer [1–3]. An important issue concerns how best to design the spacer that permits controlled transfer of electron or energy along the molecular axis. In principle, this issue can be resolved by careful manipulation of the energetics of the end-capping metal centers and the connecting spacer. In general, the design principle combines the most unsaturated form of organic linear spacer with the most stable redox- or photo-active terminals [4–21]. The design of interesting bis-2,2′:6′,2″-terpyridine ligands (tpy–tpy) by connecting two terpyridine moieties via a rigid organic spacer attached to their 4′-positions has found applications in energy conversion systems such as dye-sensitized solar cells [4] and electroluminescent devices [5]. The tpy–tpy ligands which have been reported

* Corresponding author. Tel.: +886 7 5253937; fax: +886 7 525 3908.
E-mail address: dty@mail.nsysu.edu.tw (T.-Y. Dong).

0022-328X/$ - see front matter © 2007 Elsevier B.V. All rights reserved.
doi:10.1016/j.jorganchem.2007.02.007

and used further to make dinuclear ruthenium(II) complexes are illustrated in Table 1.

Our design principle for a wire-like molecule has to fulfill following criteria: (i) organometallic redox-active spacer to enhance the capability of transfer information along the molecular axis and (ii) modular synthetic approach to control the length of the wire [21,22]. We have earlier published electrochemical and photophysical studies for a series of complexes containing bis-(2,2′:6′,2″-terpyridyl)polyferrocene redox-active spacers end-capped with photoactive Ru^{2+}–terpyridine terminals to address these issues ($[(tpy)Ru^{II}–(tpy–(fc)_n–tpy)–Ru^{II}(tpy)]^{4+}$ complexes **1a**–**c** in Scheme 1; fc = ferrocenyl; $n = 1$–3) [22]. The polyferrocenyl spacers themselves are insulators, but can be converted into semiconducting materials by selective oxidation of ferrocenyl units to form mixed-valence polyferrocenium spacers. In our earlier reports, a rapid intramolecular electron-transfer process in mixed-valence biferrocenium was observed [23]. Thus, mixed-valence polyferrocenium spacers, which possibly give an effective π-delocalization along main chain, can serve as model systems for molecular wires. The redox behavior of **1a**–**c** was dominated by the Ru^{2+}/Ru^{3+} redox couple ($E_{1/2}$ from 1.35 to 1.38 V), Fe^{2+}/Fe^{3+} redox couples ($E_{1/2}$ from 0.4 to 1.0 V) and $tpy/tpy^{-}/tpy^{2-}$ redox couples ($E_{1/2}$ from −1.3 to −1.5 V).

Table 1
Photophysical properties of the various $(tpy)Ru^{2+}$–tpy-spacer-tpyRu^{2+}(tpy) complexes at 25 °C (λ_{max}^{em}: emission maximum; Φ: emission quantum yield; τ: triplet lifetime)

Spacer	n	λ_{em}	τ (ns)	$\Phi \times 10^4$
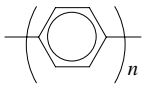	0	n.d.		
	1	n.d.		
	2	n.d.		
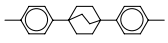		n.d.		
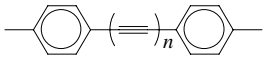	1	670	3.2	<1
	2	665	5.5	<1
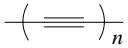	1	722	565	14
	2	735	720	23
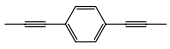		685	110	26
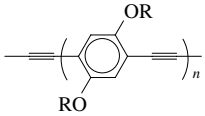	1	693	135	28
	2	695	125	25
	3	692	140	30
	4	694	130	27
	5	695	130	28
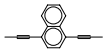		702	475	40
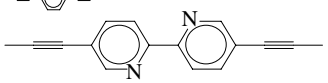		678	100	6
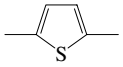		738	340	6.9
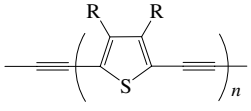	1	713	140	2.38
	2	730	164	0.42
	3	732	135	0.14
	4	726	121	0.08
	5	703	99	0.18

Attachment of ferrocenyl moiety to the 4′-position of tpy unit in the Ru^{2+} complexes has minimal influence on the Ru^{2+}/Ru^{3+} redox potential (from 1.35 to 1.38 V). These Ru^{2+}-centered oxidation processes are more positive by at least 80 mV compared to that of monomeric $[Ru(tpy)_2]^{2+}$ complex. For the binuclear Ru^{2+} complexes of tpy–$(fc)_n$–tpy, a single wave was found for the Ru^{2+}/Ru^{3+} redox couple. It might indicate that the electronic coupling between the two Ru^{2+} centers is relatively weak. Attention has also been focused on complexes illustrated in Table 1 in which a single wave of the Ru^{2+}/Ru^{3+} redox couple was also found. Recently, the physical properties of a series of linearly arranged Ru^{2+} complexes, $[(tpy)Ru^{II}–(tpy–(DEDBT)_n–tpy)–Ru^{II}(tpy)]^{4+}$ ($n = 1$, 2, 3, 4, 5), featuring Ru^{2+}–tpy chromophores connected to π-conjugated organic 2,5-diethynyl-3,4-dibutylthiophene oligomeric fragments (DEDBT), were reported [16]. The distance between two chromophoric centers was estimated from 18.5 Å ($n = 1$) to 42 Å ($n = 5$). In these diethynyl-thiophene bridged complexes, a single wave of the Ru^{2+}/Ru^{3+} redox couple was also found at ~1.36 V. The electronic coupling between the Ru^{2+} centers in the tpy–DEDBT–tpy system is also relatively weak.

In attempting to perturb the electronic properties of the spacer, we now describe an interesting example of Ru^{2+}–tpy complexes (complexes **2b**–**c** in Scheme 1) with 1,1′-bis(ethynyl)polyferrocenyl moiety attached directly to the 4′-position of tpy ligand (tpy–C≡C–$(fc)_n$–C≡C–tpy; $n = 2$–3). Complexes of **2b**–**c** have room-temperature luminescence. We expect that the insertion of ethynyl unit in the main chain could enhance the effective π-delocalization. The preparation, structural determination, and electrochemical characteristics of the Ru^{2+} free tpy–C≡C–$(fc)_n$–C≡C–tpy spacer were reported in our previous paper [24]. Spacers of tpy–C≡C–$(fc)_n$–C≡C–tpy have the capa-

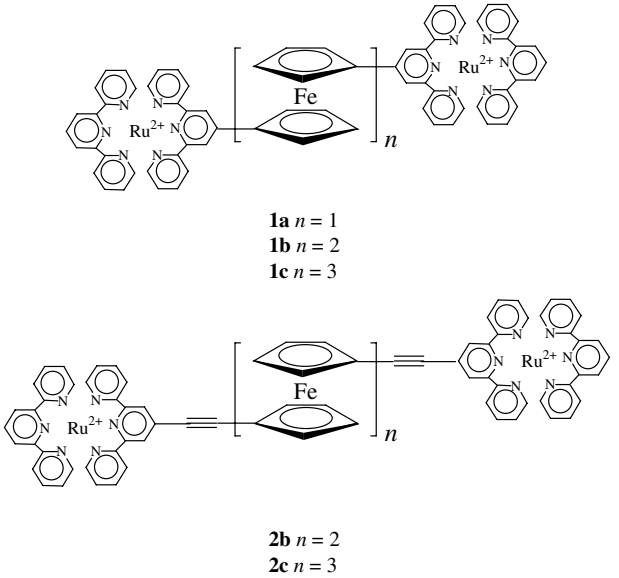

1a $n = 1$
1b $n = 2$
1c $n = 3$

2b $n = 2$
2c $n = 3$

Scheme 1. Structures of the discussed ferrocenyl-bridged Ru^{2+} complexes (counterion: PF_6^-).

bility to coordinate with transition metals, such as Ru^{2+} ion, demonstrating the versatility in molecule assembly and generation of various molecular-scale wires. To our best knowledge, no ferrocenyl-substituted binuclear Ru^{2+}–tpy molecular wire with room-temperature photoluminescent properties has been reported.

2. Results and discussion

2.1. Synthesis and characterization

Binuclear Ru(II) complexes of **2b–c** were prepared by reacting polyferrocenylalkynyl spacers (tpy–C≡C–(fc)$_n$–C≡C–tpy, fc = ferrocenyl, $n = 2$–3) with 1–1.1 equiv of $Ru(tpy)Cl_3$ (Scheme 2). The higher yields obtained in the synthesis of **2b–c**, compared to **1a–c**, prompted us to use the N–ethylmorpholine as reducing agent instead of triethylamine which was generally used to prepare $[Ru(tpy)_2]^{4+}$ derivatives [25]. Complexes were isolated as the PF_6^- salts and purified by column chromatography. All complexes were characterized by 1D and 2D NMR techniques, ESI-MS, and elemental analysis. The NMR characterization of **2b–c** in CD_3CN was achieved by utilization of ^1H–^1H and ^1H–^{13}C COSY and HMBC 2D NMR techniques. As shown in Fig. 1, the ^1H NMR spectra of **2b–c** exhibit seven signals corresponding to the tpy ligands. The spectra are characterized by the low-field doublet (appearing at 8.76 ppm) corresponding to the tpy-$H_{3',5'}$ protons and the upper-field singlet (appearing at ~8.61 ppm) corresponding to the ethynyltpy-$H_{3',5'}$ protons.

2.2. Electrochemical measurements for binuclear Ru(II)–Tpy complexes (2b–c)

The electrochemical parameters for **1a–c**, **2b–c** and related compounds obtained from the CV are summarized in Table 2. As expected, the cyclic voltammograms of **1a–c** and **2b–c** are similar. As shown in Fig. 2, the redox behavior in each of **2b–c** is dominated by the Ru^{2+}/Ru^{3+} redox couple ($E_{1/2}$ from 1.35 to 1.39 V), Fe^{2+}/Fe^{3+} redox couples ($E_{1/2}$ from 0.4 to 1.0 V) and $tpy/tpy^-/tpy^{2-}$ redox couples ($E_{1/2}$ from −1.3 to −1.5 V). Complexes **2b–c** showed reversible oxidation processes on sweeping at anodic potentials, corresponding to the oxidation of the ferrocenyl moieties, recorded at potentials from 0.0 to 1.2 V with scan

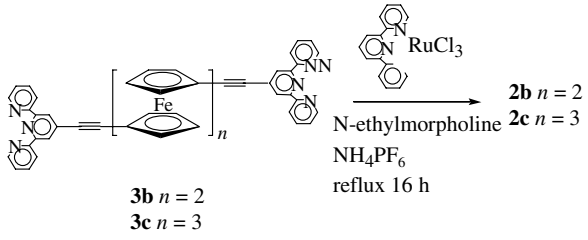

Scheme 2. Synthesis of the discussed 1,1′-bis(ethynyl)ferrocenyl-bridged Ru^{2+}–tpy complexes.

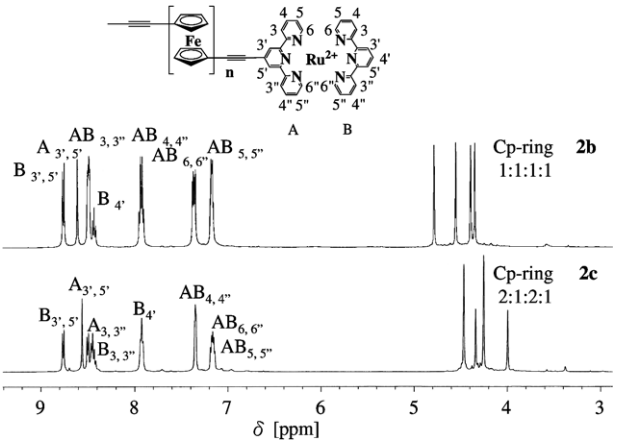

Fig. 1. ^1H NMR spectra of **2b–c** in CD_3CN.

rate of 100 mV s^{-1}. When the scanning potential was increased to 1.7 V, irreversible metal-based oxidations were developed. Furthermore, two consecutive reduction waves attributed to the reduction of the $Ru(tpy)_2^{2+}$ core were also observed.

Attachment of ethynylferrocenyl moiety to the 4′-position of tpy in Ru^{2+} complexes has minimal influence on the Ru^{2+}/Ru^{3+} redox potential (from ~1.37 to ~1.39 V). These Ru^{2+}-centered oxidation processes are more positive by at least 100 mV compared to that of $[Ru(tpy)_2]^{2+}$ complex. For the binuclear Ru^{2+} complexes of **2b–c**, a single wave was found for the Ru^{2+}/Ru^{3+} redox couple. It indicates that the electronic coupling between the two Ru^{2+} centers is relatively weak in the $[(tpy)Ru^{II}–tpy–(fc^{III})_n–tpy–Ru^{II}(tpy)]^{(n+4)+}$ state in which oxidized ferrocenium moieties are present. The electrochemical properties of a series of linearly arranged binuclear Ru^{2+} complexes given in Table 1, featuring Ru^{2+}–tpy chromophores connected to π-conjugated organic oligomeric fragments, were reported [6–19]. In these binuclear Ru^{2+}–tpy complexes, a single wave of the Ru^{2+}/Ru^{3+} redox couple was also found. The electronic coupling between the Ru^{2+} centers in each complex is relatively weak. As mentioned in the section of introduction, the distance between two chromophoric centers in $[(tpy)Ru^{II}–(tpy–(DEDBT)_n–tpy)–Ru^{II}(tpy)]^{4+}$ complexes was estimated from 18.5 Å ($n = 1$) to 42 Å ($n = 5$) [16]. In these diethynyl-thiophene bridged complexes, a single wave of the Ru^{2+}/Ru^{3+} redox couple was also found at ~1.36 V.

One of the interesting attributes of **2b** and **2c** is the magnitude of the electronic interaction between the Ru^{2+} and Fe^{2+} metal centers. Cyclic voltammetry affords a simple and effective way for estimating this interaction. If there is an interaction between the Ru^{2+} and the Fe^{2+} metal centers, the incorporation of $Ru(tpy)_2^{2+}$ units with the tpy–C≡C–(fc)$_n$–C≡C–tpy spacer (**3b–c**) would cause the Fe–Fe interactions to make any changes. It has been demonstrated that the magnitude of the peak-to-peak separation ($\Delta E_{1/2}$) gives an indication of the interaction between the metal sites in the solution state [26]. Detailed discussions

Table 2
CV data of **2b–c** and related compounds with scan rate of 100 mV s^{-1}

Compound	$Ru^{2+/3+}$	$Fe^{2+/3+}$			$Tpy^{0/1-}$
	$E_{1/2}$ (V)	$E_{1/2}$ (V)	$\Delta E_{1/2}$ (V)[a]	K_c[b] ($\times 10^{-5}$)	$E_{1/2}$ (V)
$[Ru(tpy)_2]^{2+}$[c]	1.27				−1.27
					−1.51
[Ru(tpy)(fcC≡Ctpy)]$^{2+}$[d]	1.33	0.54			−1.16
					−1.6
1a[e]	1.38	0.80			−1.17
					−1.42
1b[e]	1.35	0.61	0.31	1.8	−1.18
		0.92			−1.42
1c[e]	1.35	0.41	0.31	1.8	−1.21
		0.72	0.26		−1.46
		0.98			
3b[f]		0.60	0.38	27.6	
		0.98			
3c[f]		0.34	0.42	131.4	
		0.76	0.19		
		0.95			
2b[f]	~1.37[g]	0.50	0.33	3.9	−1.15
		0.83			−1.49
2b[e]		0.49	0.32	2.7	
		0.81			
2c[f]	~1.39[g]	0.33	0.44	286.8	−1.14
		0.77	0.15		−1.46
		0.92			
2c[e]		0.32	0.43	194.1	−1.16
		0.75			

[a] The difference of $E_{1/2}$ between two redox waves.
[b] Disproportionation constant $K_c = 10^{\Delta E(1/2)/0.059}$.
[c] From Ref. [31].
[d] fcC≡Ctpy: 4′-(ethynylferrocenyl)-2,2′:6′,2″-terpyridine. Potential is referred to the SCE in CH_2Cl_2 solution. From Ref. [35].
[e] All half-wave potentials are referred to the Ag/AgCl electrode in CH_2Cl_2/CH_3CN (1:1) solution. Under these conditions, ferrocene showed a reversible one-electron redox wave ($E_{1/2} = 0.46$ V).
[f] All half-wave potentials are referred to the Ag/AgCl electrode in CH_2Cl_2/CH_3CN (19:1) solution. Under these conditions, ferrocene showed a reversible one-electron redox wave ($E_{1/2} = 0.50$ V).
[g] Irreversible oxidation.

on the relation between $\Delta E_{1/2}$ (or K_c: disproportionation equilibrium constant) and electronic coupling can be found elsewhere [27]. Experimental $\Delta E_{1/2}$ value and calculated K_c value follow the same trend in determination of electronic coupling between metal centers. As shown in Table 2, the equilibrium constants K_c were calculated from the value of $\Delta E_{1/2}$. In the following equations, the abbreviation fc^{II} denotes the ferrocene (in Fe(II) oxidation state) unit and fc^{III} denotes ferrocenium (in Fe(III) oxidation state) unit.

$$X\text{–}fc^{II}\text{–}fc^{II}\text{–}X + X\text{–}fc^{III}\text{–}fc^{III}\text{–}X \overset{K_c}{\rightleftharpoons} 2X\text{–}fc^{II}\text{–}fc^{III}\text{–}X$$

$$X\text{–}fc^{II}\text{–}fc^{II}\text{–}fc^{II}\text{–}X + X\text{–}fc^{III}\text{–}fc^{II}\text{–}fc^{III}\text{–}X \overset{K_c}{\rightleftharpoons} 2X\text{–}fc^{II}\text{–}fc^{III}\text{–}fc^{II}\text{–}X$$

In our case there were variations detected in the potentials associated with the Fe^{2+}/Fe^{3+} redox couples in complexes of **2b–c**. The variations of the $\Delta E_{1/2}$ values (0.38 V in free spacer (**3b**) and 0.33 V in its Ru^{2+} complex (**2b**); 0.42 and 0.19 V in free spacer (**3c**) and 0.44 and 0.15 V in its Ru^{2+} complex (**2c**)) and the variations detected in the Fe^{2+}/Fe^{3+} oxidation potentials suggest that there is an interaction between the Fe^{2+} and the Ru^{2+} centers. The variation of $\Delta E_{1/2}$ values indicates that the magnitude of Fe–Fe interaction is changed on the coordination of Ru^{2+} ion. The smaller value of $\Delta E_{1/2}$ or K_c gives an indication of smaller Fe–Fe interaction. The negative potential shift of the $E_{1/2}$ values for the Fe^{2+}/Fe^{3+} redox couples upon the coordination of the Ru^{2+} ion with free spacer indicates that there is an interaction between Ru^{2+} and Fe^{2+} centers. Compared with the Ru^{2+} metal center, the ferrocenyl spacer plays a more sensitive role to gauge the interaction between the Ru^{2+} and Fe^{2+} centers. This is possible due to the existence of weak back bonding of the Fe^{2+} metal center to the tpy ligand.

A comparison of the $\Delta E_{1/2}$ of **2b** (0.33 V) and **2c** (0.44 and 0.15 V) with corresponding **1b** (0.31 V) and **1c** (0.31 and 0.26 V) indicates that the magnitude of the Fe–Fe interaction is changed by the insertion of ethynyl moiety. On the basis of data given in Table 2, insertion of ethynyl unit to the 4′-position of the tpy unit in **2b–c** complexes has only slightly influence on the Ru^{2+}/Ru^{3+} redox couple. However, the redox pontentials of the ferrocenyl moieties in **2b–c** are affected by the insertion of ethynyl unit. When

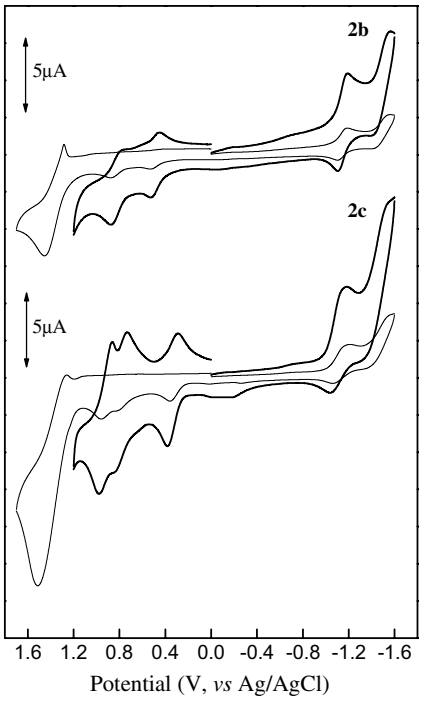

Fig. 2. Cyclic voltammetric measurements of **2b** and **2c**, recorded with a stationary glassy carbon working electrode. These experiments were carried out with a 1×10^{-3} M solution of CH_2Cl_2/CH_3CN (19:1) containing 0.2 M of $(n\text{–}C_4H_9)_4NPF_6$ as supporting electrolyte with scan rate of 0.1 V s^{-1}.

comparing individual pairs of **2b/1b** and **2c/1c**, the first Fe^{2+}/Fe^{3+} oxidation potential occurs at less negative potential, indicative of a higher HOMO energy (at 0.50 V in **2b** vs. 0.61 V in **1b**; 0.31 V in **2c** vs. 0.41 V in **1c**). Furthermore, the first tpy/tpy$^-$ reduction potential occurs at more positive potential, indicative of a lower LUMO energy (at −1.15 V in **2b** vs. −1.18 V in **1b**; −1.14 V in **2c** vs. −1.21 V in **1c**). Thus, the HOMO–LUMO energy gap is reduced by the insertion of ethynyl unit. Simultaneously, π-delocalization in the spacer is enhanced.

2.3. UV–Vis spectroscopy

The UV–Vis spectral data of **1a–c**, **2b–c**, and relevant compounds in CH_3CN are summarized in Table 3. As shown in Fig. 3, transitions occurring in the UV region ($\lambda < 350$ nm) are ascribed to the ligand-localized nature, mainly of tpy fragments. The visible absorption bands at 325 nm ($\varepsilon = 51$ M^{-1} cm^{-1}) and 440 nm ($\varepsilon = 87$ M^{-1} cm^{-1}) of ferrocene have been assigned to the $^1A_{1g} \rightarrow {}^1E_{1g}$ and $^1A_{1g} \rightarrow {}^1E_{2g}$ d–d transitions, respectively [28–30]. In comparison with ferrocene, the $^1A_{1g} \rightarrow {}^1E_{2g}$ d–d transitions of biferrocene (450 nm, $\varepsilon = 570$ M^{-1} cm^{-1}) and triferrocene (465 nm, $\varepsilon = 1900$ M^{-1} cm^{-1}) are red-shifted, and the molar absorptivity is considerably enhanced. Attachment of ethynyltpy to the ferrocenyl moiety has a significant influence on the d–d transition. The absorption bands for **3b** (496 nm, $\varepsilon = 6300$ M^{-1} cm^{-1}) and **3c** (475 nm, $\varepsilon = 4700$ M^{-1} cm^{-1}) are red-shifted relative to the biferrocene and triferrocene, and the molar absorptivities scale with the number of tpy substituents, consistent with the electron-withdrawing character of ethynyltpy [29,30].

As shown in Table 3, the visible spectra for Ru^{2+} complexes (**2b–c**) are also dominated by $^1[(d(\pi)_{Ru})^6]$

Table 3
UV–Vis absorption data[a]

Compound	Absorption data, λ_{max}/nm (ε/$\times 10^{-3}$ M^{-1} cm^{-1})
Ferrocene[b]	440(0.087), 325(0.051)
Biferrocene[c]	450(0.57), 296(7.90), 269(8.46)
Triferrocene[c]	465(1.9), 304(15), 220(65)
Terpyridine	278
fctpy[c]	459(0.91), 364(2.2), 280(28), 248(28)
bifc-tpy[c]	460(1.3), 355(sh), 285(27), 274(29), 258(43)
[Ru(tpy)(fcC≡Ctpy)]$^{2+}$[d]	525, 489(28.7), 309(81.4), 273(63.6)
$[Ru(tpy)_2][PF_6]_2$[e]	517(4.2), 472(14), 435(7.9), 308(51), 270(36)
[Ru(tpy)(fctpy)]$[PF_6]_2$[e]	515 (sh), 478(15), 306(61), 270(41)
$[Ru(fctpy)_2][PF_6]_2$[e]	526(15), 482(15), 310(60), 284(44), 274(49)
1a[f]	546(14), 519(21), 485(31), 443(18), 307(113), 273(94)
1b[f]	555(20), 525(28), 482(53), 438(30), 308(200), 270(174)
1c[f]	559(14), 526(18), 480(29), 437(17), 310(120), 273(82)
3b[g]	496(6.3), 355(sh), 291(106), 287(101), 268(132)
3c[g]	475(4.7), 367(sh), 315(44), 278(82), 250(81)
2b[g]	571(13), 529(23), 486(38), 445(21), 307(123), 273(129)
2b^{+}[g]	522(13.6), 486(30), 450(18), 312(98), 278(116)
2c[g]	579(12), 532(21), 485(34), 441(18), 310(116), 273(97)

[a] Acetonitrile solution at room temperature.
[b] From Ref. [29].
[c] From Ref. [21].
[d] From Ref. [35].
[e] See Ref. [31].
[f] From Ref. [22].
[g] This work.

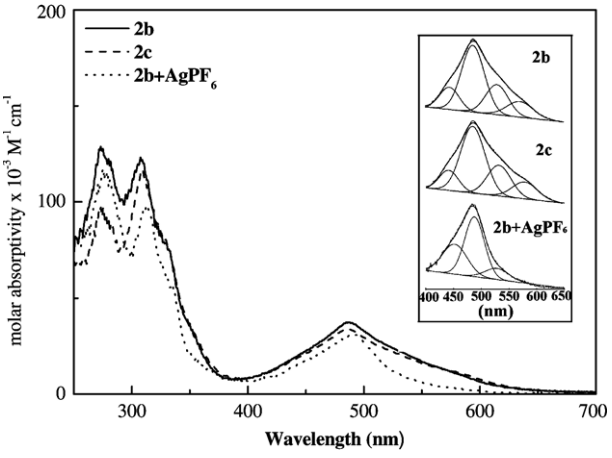

Fig. 3. UV–Vis absorption spectra of Ru^{2+} complexes **2b–c** and **2b** oxidized with $AgPF_6$. Inset: computer deconvolution for **2b–c** and **2b** oxidized with $AgPF_6$.

$\rightarrow {}^1[d(\pi)_5(\pi^*_{tpy})^1]$ MLCT absorption bands at ~485 nm which are assigned by analogy to the well-documented MLCT transitions found for $[Ru(tpy)_2]^{2+}$ (472 nm; $\varepsilon = 14\,000\ M^{-1}\,cm^{-1}$), $[Ru(tpy)(fctpy)]^{2+}$ (478 nm; $\varepsilon = 15\,000\ M^{-1}\,cm^{-1}$), $[Ru(tpy)(fcC{\equiv}Ctpy)]^{2+}$ (489 nm; $\varepsilon = 28\,700\ M^{-1}\,cm^{-1}$), and $[Ru(fctpy)_2]^{2+}$ (482 nm, $\varepsilon = 15\,000\ M^{-1}\,cm^{-1}$) [31–35]. The MLCT bands at 486 nm ($\varepsilon = 38\,000\ M^{-1}\,cm^{-1}$) for **2b** and at 485 nm ($\varepsilon = 34\,000\ M^{-1}\,cm^{-1}$) for **2c** are slightly blue-shifted relative to the monomeric $[Ru(tpy)(fcC{\equiv}Ctpy)]^{2+}$ complex [35], and the molar absorptivities are considerably enhanced. The absorption bands are broad because they include a series of MLCT transitions. Computer deconvolution of the MLCT band with four Gaussian lines was carried out. The resulting fitting curves are collected in Table 3 and shown in Fig. 3. Well-defined shoulders at both high and low-energy regions of the Ru^{2+}-to-tpy MLCT band were observed for the monomeric $[Ru(tpy)_2]^{2+}$ and **2b–c**. In the case of $[Ru(tpy)_2]^{2+}$, these shoulders were previously assigned to ${}^1[(d(\pi)_{Ru})^6] \rightarrow {}^3[d(\pi)^5(\pi^*_{tpy})^1]$ MLCT which become partially allowed due to the spin-orbital coupling, which has the effect of mixing the singlet and triplet excited-state manifolds [33,34]. Compared with $[Ru(tpy)_2]^{2+}$, the molar absorptivities of these shoulders at ~530 and ~440 nm in the case of **2b** and **2c** are quite stronger. Here, we do not have reasonable explanation for the increasing of molar absorptivity. However, we believe that the Ru^{2+}-to-tpy MLCT can be attributed to these shoulders.

Closer inspection has revealed that the UV–Vis spectra of **2b–c** exhibit a shoulder on the low-energy side. As shown in Fig. 3, from computer deconvolution absorption bands at 571 nm ($\varepsilon = 13\,000\ M^{-1}\,cm^{-1}$) for **2b**, and at 579 nm ($\varepsilon = 12\,000\ M^{-1}\,cm^{-1}$) for **2c** are apparent in the visible region. In the case of Ru^{2+} transition metal complexes containing ferrocenyl moiety, an intense broad structureless band in the 520 nm region has been observed [2,31,36]. For the $[Ru(fctpy)_2]^{2+}$ and $[Ru(tpy)(fcC{\equiv}Ctpy)]^{2+}$ complexes, bands at 526 and 525 nm were observed, respectively [31,35]. On the basis of resonance Raman study, this band has been assigned to the ferrocene-based ${}^1[(d(\pi)_{Fe})^6] \rightarrow {}^1[(d(\pi)_{Fe})^5(\pi^{*Ru}_{tpy})^1]$ MLCT [31]. The intensity of this transition scales with the number of ferrocenyl substituents and it disappears upon the oxidation of ferrocene. In our studies, this band is not present in the parent Ru^{2+}-free spacers (**3b–c**), but on the coordination with Ru^{2+} metal centers rises to a red-shifted and more intense transition in the visible region for **2b** and **2c** relative to the $[Ru(fctpy)_2]^{2+}$ and $[Ru(tpy)(fcC{\equiv}Ctpy)]^{2+}$ complexes. Furthermore, this band disappears upon the oxidation of ferrocene unit in **2b** with $AgPF_6$. The observed red-shifted absorption from ~525 nm in monomeric $[Ru(fctpy)_2]^{2+}$ and $[Ru(tpy)(fcC{\equiv}Ctpy)]^{2+}$ complexes to ~570 nm in **2b** and **2c** and a concomitant increase of the intensity of this band indicate that there is a qualitative electronic coupling within the ferrocenyl array. This is consistent with the electrochemical behavior discussed above. We suggest that the filled $3d_{x^2-y^2,xy,z^2}$ and empty $3d_{xz,yz}$ orbitals on each Fe^{2+} ion would overlap with each other resulting from Fe–Fe interactions, leading to absorption band in a red characteristic of the ${}^1[(d(\pi)_{Fe})^6] \rightarrow {}^1[(d(\pi)_{Fe})^5(\pi^{*Ru}_{tpy})^1]$ MMLCT (metal–metal-to-ligand charge transition) [22].

Comparing the λ_{max} of the molecular wires of **2b–c** with **1a–c**, it is noted that the ${}^1[(d(\pi)_{Fe})^6] \rightarrow {}^1[(d(\pi)_{Fe})^5(\pi^{*Ru}_{tpy})^1]$ transition in **2b–c** occurs at a larger red shift of ~15 nm after the insertion of ethynyl unit in the main chain. The insertion of the ethynyl group into the main chain causes a substantial increase in the magnitude of electronic coupling between Ru^{2+} and Fe^{2+} centers. Comparison of the photophysical properties observed for **2b–c** with **1a–c** suggests more pronounced electron delocalization in the complexes of **2b–c**. Indeed, the ${}^1[(d(\pi)_{Fe})^6] \rightarrow {}^1[(d(\pi)_{Fe})^5(\pi^{*Ru}_{tpy})^1]$ transitions are more red-shifted and triplet lifetimes are significantly longer for **2b–c** than those for **1a–c**. The insertion of ethynyl group influences the strength of electronic coupling between metal centers and tpy–Cp linkage.

2.4. Photophysical properties

As given in Table 4, in deoxygenated pure CH_3CN or H_2O/CH_3CN (4/1) solution at 25 °C, the complexes of **1a–c** ($\lambda_{exc} = 480$–580 nm) are nonemissive. Because electronic coupling between the Ru^{2+} and ferrocenyl center is small, attachment of a ferrocene moiety to the 4′-position of tpy has minimal influence on the photophysical properties in comparison with the monomeric components. Complex of $[Ru(tpy)_2]^{2+}$ exhibits rather short ^{3}MLCT excited-state lifetime (250 ps) at room temperature. The $[Ru(tpy)(fctpy)]^{2+}$ and $[Ru(fctpy)_2]^{2+}$ complexes are nonemissive in room-temperature fluid solution [31]. The excited-state lifetime measurements indicated an upper-limit emission lifetime of 25 ns (λ^{em}_{max} at 600 nm) in 4:1 EtOH/MeOH (v/v) at 77 K, substantially shorter than that found for $Ru(tpy)_2^{2+*}$ ($\tau = 11$ μs) at 77 K [36]. The very short lifetimes

Table 4
Room-temperature luminescence data

Compound	Emission (nm)[a]			k_r ($\times 10^{-3}$, s^{-1})[b]	k_{nr} ($\times 10^{-7}$, s^{-1})[b]
	λ_{max}	Φ ($\times 10^4$)	τ (ns)		
$[Ru(tpy)_2]^{2+}$	n.d.				
1a	n.d.				
1b	n.d.				
1c	n.d.				
2b	690	1.48	67	2.2	1.5
2b$^+$	n.d.				
2c	690	1.13	24	4.7	4.2
3b	n.d.				
3c	n.d.				

[a] In H_2O/CH_3CN (4/1) solution at room temperature (λ_{max}: emission maximum and Φ: emission quantum yield (measured at $\lambda_{exc} = 490$ nm); τ: triplet lifetime (measured at $\lambda_{exc} = 340$ nm)). n.d.: non-detectable.

[b] From $\Phi = k_{nr}/(k_{nr} + k_{nr})$ where k_r and k_{nr} represenr the rate constants for radiative and nonradiative decay with$k_r = \Phi/\tau$ and $k_{nr} = 1/\tau - k_r$.

observed for $[Ru(tpy)(fctpy)]^{2+}$ and $[Ru(fctpy)_2]^{2+}$ ^{3}MLCT excited states at 77 K have been attributed to the presence of ferrocenyl moiety which provides additional channels for excited-states deactivation. The ferrocenyl moiety acts as efficient quencher for the ^{3}MLCT state. Very recently, the photophysical properties of $[Ru(tpy)(fcC{\equiv}Ctpy)]^{2+}$ and $[Ru(fcC{\equiv}Ctpy)_2]^{2+}$ in aqueous H_2O/CH_3CN (4/1) solution were described by Siemeling et al., who found [35] the first example of monomeric ferrocenyl-substituted Ru^{2+} complex showing room-temperature luminescence. Complex of $[Ru(fcC{\equiv}Ctpy)_2]^{2+}$ containing two ferrocenyl units showed no luminescence at 77 K in H_2O/CH_3CN (4/1) solution frozen solution, whereas complex of $[Ru(tpy)(fcC{\equiv}Ctpy)]^{2+}$ containing one ferrocenyl unit was weakly emissive at room temperature (λ_{max}^{em} at 699 nm with emission quantum yield (Φ): 0.0004; ^{3}MLCT lifetime (τ): 260 ns). To our best knowledge, no binuclear Ru^{2+}–tpy molecular wire containing ferrocenyl-substituted spacer with room-temperature photoluminescent properties has been reported. As shown in Table 1, complexes containing unsaturated form of organic linear spacers end-capped by Ru^{2+} metal centers also showed room-temperature photoluminescent properties.

Interestingly, the insertion of ethynyl group into the main chain, giving **2b** and **2c**, respectively, causes a dramatic increase of luminescence quantum yields (1.48×10^{-4} for **2b**; 1.13×10^{-4} for **2c**), triplet lifetimes (67 ns for **2b**; 24 ns for **2c**), and emission maximum (690 nm for **2b**–**c**; Fig. 4 and Table 4). Fig. 4 shows the emission spectra of **2b**–**c** and **2b**$^+$. Emission in pure acetonitrile is extremely weak. Furthermore, the emission spectra have the same spectral shape regardless of the excitation wavelength and differ only in intensity. The single, symmetric emission band at $\lambda_{max} = 690$ nm indicates that a single excited state is responsible for the emission observed. As shown in Fig. 5, a detailed comparison was made between the absorption spectrum and excitation spectrum and the spectra were plotted with the restriction that the absorption spectrum must be higher in intensity than the excitation spectrum. The maximum of the excitation spectrum is red-shifted. Furthermore, the low-energy shoulder assigned to the $^1[(d(\pi)_{Fe})^6] \rightarrow {}^1[(d(\pi)_{Fe})^5(\pi^{*Ru}_{tpy})^1]$ transition (ferrocenyl-based MLCT) at ~570 nm can be observed in both absorption and excitation spectra. This is unexpected, since relevant ferrocenyl derivatives are known to be nonluminescent. In the case of monomeric $[Ru(tpy)(fcC{\equiv}Ctpy)]^{2+}$, the $^1[(d(\pi)_{Fe})^6] \rightarrow {}^1[(d(\pi)_{Fe})^5(\pi^{*Ru}_{tpy})^1]$ transition was observed in the absorption spectrum, but not in the excitation spectrum [35]. Siemeling et al. have suggested that it is not exhibited a decay pathway from the $^1[Ru^{II}–tpy^-–fc^{III}]$ excited state to the $^3[Ru^{III}–tpy^-–fc^{II}]$ luminescent excited-state in the case of monomeric $[Ru(tpy)(fcC{\equiv}Ctpy)]^{2+}$ complex. In our case, we would like to suggest that it is possible to decay from the $^1[Ru^{II}–tpy^-–fc^{III}–fc^{II}–tpy–Ru^{II}]$ excited state to the $^3[Ru^{III}–tpy^-–fc^{II}–fc^{II}–tpy–Ru^{II}]$ luminescent excited-state (see Fig. 6).

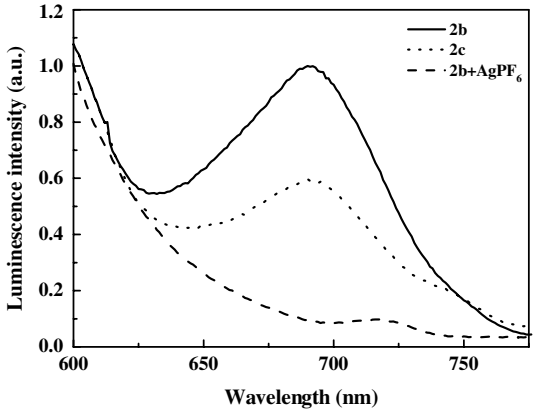

Fig. 4. Luminescence spectra at $\lambda_{exc} = 490$ nm of the indicated complexes in H_2O/CH_3CN (4/1) solution at room temperature.

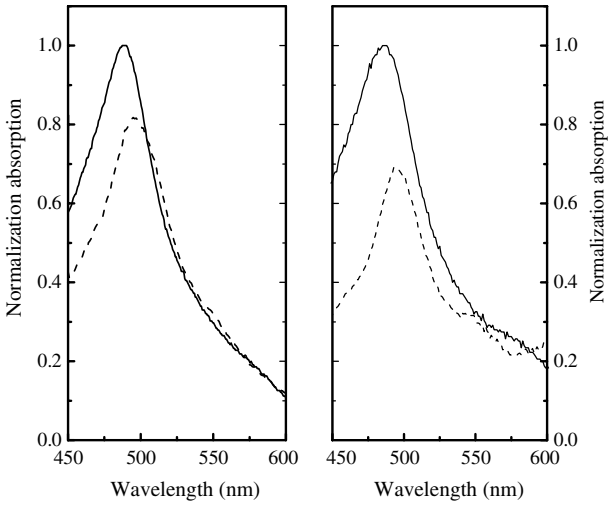

Fig. 5. Comparsion of absorption spectrum (solid) in CH_3CN solution and excitation spectrum (dashed) in H_2O/CH_3CN (4/1) solution for **2b** (left) and **2c** (right).

When comparing the values of Φ and τ of **2c** with that of **2b**, we indeed observed that **2c** is weakly emissive, because three ferrocenyl moieties in **2c** are present, instead of two in **2b**. This finding is in line with the general observation that ferrocenyl unit acta as efficient quencher. The binuclear complexes **2b**–**c** also show decreased triplet energies in comparison with the mononuclear $[Ru(tpy)(fctpy)]^{2+}$ and $[Ru(fctpy)_2]^{2+}$. The increase of luminescence yields and triplet lifetimes observed for **2b**–**c** relative to **1a**–**c** is attributed to the more pronounced electron delocalization in the extended π^* orbitals. The electron is excited to the ethynyl-substituted tpy ligand where it is delocalized over the extended π-electron system that includes ferrocenyl subunits.

The biferrocenyl spacer can be converted into mixed-valence biferrocenium spacer, which gives a more effective π-delocalization along main chain, by selective chemical oxidation of ferrocenyl unit. The ferrocenyl subunit in complex **2b** was oxidized to form a mixed-valence complex (**2b**$^+$), containing one ferrocenium Fe^{3+}-center, with 1

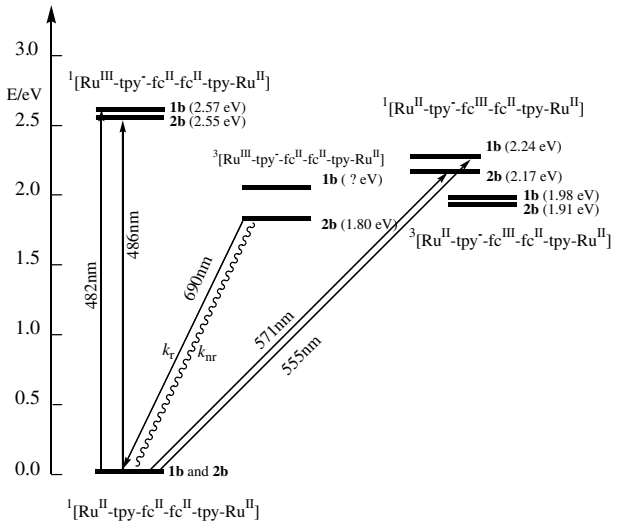

Fig. 6. Excited-state energy level diagram for **1b** and **2b**.

equiv. amount of $AgPF_6$. As shown in Fig. 3, it is noted that the $^1[(d(\pi)_{Fe})^6] \rightarrow {}^1[(d(\pi)_{Fe})^5(\pi^{*Ru}_{tpy})^1]$ band disappears in the UV–Vis spectral data of $\mathbf{2b}^+$. Furthermore, the presence of the $^1[(d(\pi)_{Ru})^6] \rightarrow {}^1[d(\pi)^5(\pi^*_{tpy})^1]$ band with same intensity (485 nm; $\varepsilon = 1.2 \times 10^4\ M^{-1}\,cm^{-1}$) indicates the ruthenium centers are in Ru^{2+} oxidation state. In deoxygenated H_2O/CH_3CN (4/1) solution at 25 °C, the complex of $\mathbf{2b}^+$ ($\lambda_{exc} = 490$ nm) is nonemissive (Fig. 4).

In the case of monomeric $[Ru(tpy)(fcC{\equiv}Ctpy)]^{2+}$ complex, Siemeling et al. reported [35] that oxidation of the ferrocenyl moiety leads to an increase in emission intensity. Siemeling et al. suggested that in this case ferrocenium quenching is no longer possible. The oxidized $[Ru(tpy)(fcC{\equiv}Ctpy)]^{3+}$ complex gave essentially the same ^{3}MLCT lifetime (τ: 250 ns). This indicates that the MLCT excited-state is independent of the ferrocenyl unit. In our case mixed-valence ferrocenium unit still plays an efficient quencher for the MLCT excited-state. Excited-states of $[Ru^{III}_a$–tpy$^-$–fc^{II}–fc^{III}–tpy–$Ru^{II}_b]$ and $[Ru^{III}_a$–tpy$^-$–fc^{III}–fc^{II}–tpy–$Ru^{II}_b]$ are energetically degenerated, resulting form the rapid electron-transfer process between two Fe^{2+} and Fe^{3+} centers. In our earlier reports [23], the rate of intramolecular electron-transfer in mixed-valence biferrocenium cations in solution state was estimated to be $>\sim 10^{12}\ s^{-1}$ (τ: <1 ps). The presence of lower energy ferrocenium-centered $[Ru^{II}_a$–tpy$^-$–fc^{III}–fc^{III}–tpy–$Ru^{II}_b]$ state provides an additional channel for excited-states decay. The mixed-valence biferrocenium center acts as an efficient quencher for the MLCT excited-state.

2.5. MLCT excited-state decay

When comparing the photophysical properties in **2b–c** with **1a–c**, we indeed observed that the insertion of ethynyl group into the main chain, giving **2b** and **2c**, respectively, causes a dramatic increase of phosphorescence yield, triplet lifetime, and emission intensity. We suggest that the insertion of ethynyl group into the main chain to perturb the electronic properties of the spacer causes more pronounced electron delocalization in the extended π^* orbitals. As shown in Fig. 6, the enhanced luminescence yield and triplet lifetime observed for **2b–c** relative to **1a–c** can be illustrated with a comprehensive excited-state energy level diagram, showing the Ru^{2+}–tpy-based states on the left and the expected ferrocene-based states on the right. Using UV spectroscopic data of $^1[(d(\pi)_{Ru})^6] \rightarrow {}^1[d(\pi)^5(\pi^*_{tpy})^1]$ and $^1[(d(\pi)_{Fe})^6] \rightarrow {}^1[(d(\pi)_{Fe})^5(\pi^{*Ru}_{tpy})^1]$ MLCT bands, the excited-state energies of $^1[Ru^{III}$–tpy$^-$–fc^{II}–fc^{II}–tpy–$Ru^{II}]$ (2.57 eV in **1b** and 2.55 eV in **2b**) and $^1[Ru^{II}$–tpy$^-$–fc^{III}–fc^{II}–tpy–$Ru^{II}]$ (2.24 eV in **1b** and 2.17 eV in **2b**) are estimated. The excited-state energy of $^3[Ru^{III}$–tpy$^-$–fc^{II}–fc^{II}–tpy–$Ru^{II}]$ in **2b** is estimated to be 1.80 eV from the emission maximum (690 nm). Because complex of **1b** is non-emissive, the excited-state energy of $^3[Ru^{III}$–tpy$^-$–fc^{II}–fc^{II}–tpy–$Ru^{II}]$ in **1b** cannot be estimated. However, the excited state of $^3[Ru^{II}$–tpy$^-$–fc^{III}–fc^{II}–tpy–$Ru^{II}]$ in **1b** can provide an additional decay pathway. Therefore, we would suggest that the $^3[Ru^{III}$–tpy$^-$–fc^{II}–fc^{II}–tpy–$Ru^{II}]$ excited-state energy in **1b** should be greater than the energy of $^3[Ru^{II}$–tpy$^-$–fc^{III}–fc^{II}–tpy–$Ru^{II}]$ excited-state in **1b**. The lower lying $^1[Ru^{III}$–tpy$^-$–fc^{II}–fc^{II}–tpy–$Ru^{II}]$, $^1[Ru^{II}$–tpy$^-$–fc^{III}–fc^{II}–tpy–$Ru^{II}]$, and $^3[Ru^{III}$–tpy$^-$–fc^{II}–fc^{II}–tpy–$Ru^{II}]$ excited states in **2b–c** relative to **1a–c** are expected. Insertion of ethynyl group has less influence on the energy of $^1[Ru^{III}$–tpy$^-$–fc^{II}–fc^{II}–tpy–$Ru^{II}]$ state. For $^1[Ru^{III}$–tpy$^-$–fc^{II}–fc^{II}–tpy–$Ru^{II}]$ excited state, the energy difference between **1b** and **2b** is only ~0.02 eV. On the basis of $^1[(d(\pi)_{Fe})^6] \rightarrow {}^1[(d(\pi)_{Fe})^5(\pi^{*Ru}_{tpy})^1]$ transition, insertion of ethynyl group has more influence on the $^1[Ru^{II}$–tpy$^-$–fc^{III}–fc^{II}–tpy–$Ru^{II}]$ electronic state of **2b**. For $^1[Ru^{II}$–tpy$^-$–fc^{II}–fc^{III}–tpy–$Ru^{II}]$ excited state, the energy difference between **1b** and **2b** is ~0.07 eV. Excited-state upper limiting energies of $^3[Ru^{II}$–tpy$^-$–fc^{III}–fc^{II}–tpy–$Ru^{II}]$ in **1b** and **2b** are estimated to be 1.98 and 1.91 eV, respectively, from the low-energy onset of the $^1[(d(\pi)_{Fe})^6] \rightarrow {}^1[(d(\pi)_{Fe})^5(\pi^{*Ru}_{tpy})^1]$ MLCT band [36]. Here, we would like to suggest that the insertion of ethynyl group caused more pronounced electron delocalization in the extended π^* orbitals has more influence on the $^3[Ru^{III}$–tpy$^-$–fc^{II}–fc^{II}–tpy–$Ru^{II}]$ excited state of **2b**. Because of its larger decrease in energy, there will be less pronounced mixing between the lower energy $^3[Ru^{III}$-tpy$^-$–fc^{II}–fc^{II}–tpy–$Ru^{II}]$ state and the higher energy $^3[Ru^{II}$–tpy$^-$–fc^{III}–fc^{II}–tpy–$Ru^{II}]$ state in **2b**. Therefore, complexes of **2b–c** have room-temperature luminescence in H_2O/CH_3CN (4/1) solution. In the case of mixed-valence $\mathbf{2b}^+$, the lowest lying excited state is expected to be $[Ru^{II}$–tpy$^-$–fc^{III}–fc^{III}-tpy–$Ru^{II}]$ state. From the deactivation of $\mathbf{2b}^+$, the $[Ru^{II}$–tpy$^-$–fc^{III}–fc^{III}-tpy–$Ru^{II}]$ state can provide an additional channel for excited-states decay.

3. Conclusion

Summarizing, we have systematically undertaken the electrochemical and photophysical studies to probe elec-

tronic states for a series of complexes containing bis-(2,2′:6′,2″-terpyridyl)polyferrocene redox-active spacers end-capped with photoactive Ru^{2+}–terpyridine terminals. The ground-state HOMO and LUMO energies are estimated from electrochemical measurements. When comparing individual pairs of **2b/1b** and **2c/1c**, the insertion of ethnyl group results in an increase of HOMO energy and a decrease of LUMO energy. Oxidation potentials of the ferrocenyl moieties and the tpy reduction potentials are matched as closely as possible, and π-delocalization in the spacer is enhanced. Complexes of **1a–c** show no room-temperature luminescence. Complexes of **2b–c** containing an ethynyl unit attached to the tpy ligand are emissive at room-temperature in H_2O/CH_3CN (4/1) solution. We have found that the insertion of ethynyl group into the main chain can lead to an increase in excited-state lifetimes (67 ns for **2b** and 24 ns for **2c**), which is due to the strong electronic coupling between the π systems of the tpy ligand and the ethynyl unit. The biferrocenyl spacer can be converted into mixed-valence biferrocenium spacer, which gives a more effective π-delocalization along main chain. The ferrocenyl subunit in complex **2b** was oxidized to form a mixed-valence complex ($\mathbf{2b}^+$). In deoxygenated H_2O/CH_3CN (4/1) solution at 25 °C, the complex of $\mathbf{2b}^+$ ($\lambda_{exc} = 490$ nm) is nonemissive. Oxidation of the ferrocenyl spacer enhances the quenching pathway.

4. Experimental

4.1. Genera information

All manipulations involving air-sensitive materials were carried out by using standard Schlenk techniques under the atmosphere of N_2. Solvents were dried as follows: THF and ether were distilled from Na/benzophenone; CH_2Cl_2 was distilled from CaH_2; diisopropylamine and TMEDA were distilled from KOH. As shown in Scheme 2, complexes **2b–c** could be prepared. Preparations of the polyferrocenylalkyne spacers (tpy–C≡C–$(fc)_n$–C≡C–tpy, fc = ferrocenyl, $n = 2$–3) were described in our previous paper [24].

4.2. Preparation of compounds *2b–c*

An ethanol (30 ml) solution of corresponding**3b** (40.0 mg, 0.0455 mmol) or **3c** (50.0 mg, 0.0470 mmol), stoichiometric amount of $RuLCl_3$ (L = 2,2′:6′,2″-terpyridine) [25] and 10 drops of *N*-ethylmorpholine was heated to reflux for 16 h. After cooling the reaction mixture, the volume of ethanol solvent was reduced to one-half. An aqueous solution of NH_4PF_6 was added to give a violet-blue precipitate which was collected by filtration. In the case of **2b**, the crude product was chromatographed on act. V Al_2O_3, eluting with CH_2Cl_2. The first band was starting material. Continued elution with CH_3OH/acetone (5: 95) afforded compound **2b** which was recrystallized from acetone/ether (1:1). In the case of **2c**, the crude product was purified directly by recrystallization from acetone/ether (1:1). The yield of **2b** was 0.0197 g (20%).^{1}H NMR (acetonitrile-d_3) of **2b**: δ 8.76 (d, 8.5 Hz, 4H, tpy-$H_{3',5'}$); 8.61 (s, 4H, ethynyltpy-$H_{3',5'}$); 8.50 (d, 3 Hz, 4H, tpy-$H_{3,3''}$); 8.48 (d, 3 Hz, 4H, ethynyltpy-$H_{3,3''}$); 8.43 (t, 8.2 Hz, 2H, tpy-$H_{4'}$); 7.94 and 7.92 (dd, 8 Hz; 8 Hz, 8H, ethynyltpy and tpy-$H_{4,4''}$); 7.38 and 7.36 (d, 5.5 Hz, 8H, ethynyltpy and tpy-$H_{6,6''}$); 7.18 and 7.16 (dd, 8 Hz; 5.5 Hz, 8H, ethynyltpy and tpy-$H_{5,5''}$); 4.79 (s, 4H, Cp); 4.56 (s, 4H, Cp); 4.40 (s, 4H, Cp); 4.35 (s, 4H, Cp). Mass spectrum of **2b** (ESI): 920.09 (calcd. 920.56 for $[M-2PF_6]^{2+}$); 565.06 (calcd. 565.72 for $[M-3PF_6]^{3+}$); 387.55 (calcd. 388.30 for $[M-4PF_6]^{4+}$). Anal. Calc. for **2b** ($C_{84}H_{58}F_{24}Fe_2N_{12}P_4Ru_2$ MW 2129.16264): C, 47.39; H, 2.75; N, 7.89. Found: C, 46.94; H, 3.02; N, 7.52%. The yield of **2c** was 0.0329 g (30%). ^{1}H NMR (acetonitrile-d_3) of **2c**: δ 8.76 (d, 8.5 Hz, 4H, tpy-$H_{3',5'}$); 8.56 (s, 4H, ethynyltpy-$H_{3',5'}$); 8.50 (d, 8 Hz, 4H, ethynyltpy-$H_{3,3''}$); 8.45 (d, 8.5 Hz, 4H, tpy-$H_{3,3''}$); 8.43 (t, 8.5 Hz, 2H, tpy-$H_{4'}$); 7.92 (t, 6.8 Hz, 8H, ethynyltpy and tpy-$H_{4,4''}$); 7.35 (br, 8H, ethynyltpy and tpy-$H_{6,6''}$); 7.16 (m, 8H, ethynyltpy and tpy-$H_{5,5''}$); 4.47 (s, 8H, Cp); 4.34 (s, 4H, Cp); 4.25 (s, 8H, Cp); 4.00 (s, 4H, Cp). Mass spectrum of **2c** (ESI): 1012.03 (calcd. 1012.56 for $[M-2PF_6]^{2+}$); 626.48 (calcd. 627.05 for $[M-3PF_6]^{3+}$); 433.79 (calcd. 434.30 for $[M-4PF_6]^{4+}$). Anal. Calc. for **2c** ($C_{94}H_{66}F_{24}Fe_3N_{12}P_4Ru_2$ MW 2313.18364): C, 48.81; H, 2.88; N, 7.27. Found: C, 48.69; H, 2.96; N, 6.92%.

4.3. Physical measurement

^{1}H NMR spectra were run on a Varian INOVA-500 MHz spectrometer. Mass spectra were obtained with a VG-BLOTECH-QUATTRO 5022 system and ESI-LCQ mass spectra were obtained with a Thermo Finnigan spectroscopy. Electrochemical measurements were carried out with a CHI 660B system. For complexes of **2b–c**, cyclic voltammetry measurements were performed with a stationary glassy carbon working electrode. These experiments were carried out with a 1×10^{-3} M solution of CH_2Cl_2/CH_3CN (19:1) containing 0.2 M of $(n\text{–}C_4H_9)_4NPF_6$ as supporting electrolyte. The potentials quoted in this work were relative to the Ag/AgCl electrode at 25 °C. Under these conditions, ferrocene showed a reversible one-electron redox wave ($E_{1/2} = 0.50$ V). Emission spectra were measured with a Hitachi F4500 photon-counting spectrofluorometer equipped with a red-sensitive R928F photomultiplier tube. Wavelength was corrected using $[Ru(bpy)_3]^{2+}$ as reference standard ($\lambda_{max}^{em} = 607$ nm). Luminescence quantum yields (Φ) were measured ($\lambda_{exc} = 490$ nm) in optically dilute H_2O/CH_3CN (4/1) solution (5×10^{-6} M) at room temperature by comparing wavelength-integrated intensities (I) with reference to $[Ru(bpy)_3][PF_6]_2$ ($\Phi = 0.059$ in H_2O/CH_3CN (4/1) solution) as standard and by using the following equation: where A and η are absorbance values at the employed excitation wavelength and refractive index of the solvent, respectively:

$$\Phi/\Phi_r = A_r\eta^2 I/A\eta_r^2 I_r$$

Luminescence lifetimes were measured by OB920 time resolved fluorescence spectroscopy with nF-900 Nanosecond Flashlamp (Edinburgh Instruments Ltd.) with a time-correlated, single-photon counting methodology following excitation at 340 nm. UV spectra were recorded from 250 to 800 nm in CH_3CN by using 1.0 cm quartz cells with a Hitachi U-4001 spectrophotometer.

Acknowledgements

We thank the National Science Council, Department of Chemistry and Center for Nanoscience and Nanotechnology at National Sun Yat-Sen University.

Appendix A. Supplementary material

^{13}C NMR spectra and ESI-mass spectra of **2b** and **2c** are included. Supplementary data associated with this article can be found, in the online version, at doi:10.1016/j.jorganchem.2007.02.007.

References

[1] V. Balzani, F. Scandola, Supramolecular Photochemistry, Ellis Horwood, Chichester, 1991.
[2] (a) J.-P. Sauvage, J.-P. Collin, J.-C. Chambron, S. Guillerez, C. Coudret, V. Balzani, F. Barigolletti, L. De Cloa, L. Flamigni, Chem. Rev. 94 (1994) 993;
(b) A. Harriman, R. Ziessel, Coord. Chem. Rev. 171 (1998) 331;
(c) F. Barigelletti, L. Flamigni, Chem. Soc. Rev. 29 (2000) 1.
[3] J.-P. Collin, P. Gaviña, V. Heitz, J.-P. Sauvage, Eur. J. Inorg. Chem. 1 (1998) 1.
[4] (a) A. Hagfeldt, M. Grätzel, Acc. Chem. Res. 33 (2000) 269;
(b) C.A. Bignozzi, R. Argazzi, C.J. Kleverlaan, Chem. Soc. Rev. 29 (2000) 87;
(c) P. Wang, S.M. Zakeeruddin, J.E. Moser, M.K. Nazeeruddin, T. Sekiguchi, M. Grätzel, Nat. Mater. 2 (2003) 402;
(d) A. Islam, H. Sugihara, H. Arakawa, J. Photochem. Photobiol. A 158 (2003) 131.
[5] (a) J. Slinker, D. Bernards, P.L. Houston, H.D. Abruna, S. Bernhard, G.G. Malliaras, Chem. Commun. (2003) 2392;
(b) G. Kalyuzhny, M. Buda, J. Mcneill, P. Barbara, A.J. Bard, J. Am. Chem. Soc. 125 (2003) 6272;
(c) S. Welter, K. Brunner, J.W. Hofstraat, L. De Cola, Nature 421 (2003) 54.
[6] M.T. Indelli, F. Scandola, J.-P. Collin, J.-P. Sauvage, A. Sour, Inorg. Chem. 35 (1996) 303.
[7] C. Patoux, J.-P. Launay, M. Beley, S. Chodorowski-Kimmes, J.-P. Collin, S. James, J.-P. Sauvage, J. Am. Chem. Soc. 120 (1998) 3717.
[8] M. Beley, S. Chodorowski-Kimmes, J.-P. Collin, P. Lainé, J.-P. Launay, J.-P. Sauvage, Angew. Chem., Int. Ed. Engl. 33 (1994) 1775.
[9] M. Schütte, D.G. Kurth, M.R. Linford, H. Cölfen, H. Möhwald, Angew. Chem., Int. Ed. Engl. 37 (1998) 2891.
[10] L. Hammarström, F. Barigelletti, L. Flamigni, N. Armaroli, A. Sour, J.-P. Collin, J.-P. Sauvage, J. Am. Chem. Soc. 118 (1996) 11972.
[11] V. Grosshenny, A. Harriman, J.-P. Gisselbrecht, R. Ziessel, J. Am. Chem. Soc. 118 (1996) 10315.
[12] A.C. Benniston, V. Grosshenny, A. Harriman, R. Ziessel, Angew. Chem., Int. Ed. Engl. 33 (1994) 1884.
[13] V. Grosshenny, A. Harriman, R. Ziessel, Angew. Chem., Int. Ed. Engl. 34 (1995) 2705.
[14] V. Grosshenny, A. Harriman, R. Ziessel, Angew. Chem., Int. Ed. Engl. 34 (1995) 1100.
[15] A. El-ghayoury, A. Harriman, A. Khatyr, R. Ziessel, Angew. Chem., Int. Ed. Engl. 39 (2000) 185.
[16] (a) A. Harriman, A. Mayeux, A. De Nicola, R. Ziesel, Phys. Chem. Chem. Phys. 4 (2002) 2229;
(b) A. Barbieri, B. Ventura, F. Barigletti, A. De Nicola, M. Quesada, R. Ziessel, Inorg. Chem. 43 (2004) 7359;
(c) J. Hjelm, R.W. Handel, A. Hagfeldt, E.C. Constable, C.E. Housecroft, R.J. Forster, Inorg. Chem. 44 (2005) 1073.
[17] M. Hissler, A. El-ghayoury, A. Harriman, R. Ziessel, Angew. Chem., Int. Ed. Engl. 37 (1998) 1717.
[18] A. Harriman, A. Khatyr, R. Ziessel, A.C. Benniston, Angew. Chem., Int. Ed. Engl. 39 (2000) 4287.
[19] F. Barigelletti, L. Flamigni, G. Calogero, L. Hammarström, J.-P. Sauvage, J.-P. Collin, Chem. Commun. (1998) 2333.
[20] S. Flores-Torres, G.R. Hutchison, L.J. Soltzberg, H.D. Abruna, J. Am. Chem. Soc. 128 (2006) 1513.
[21] T.-Y. Dong, M.C. Lin, Y.N.M. Chiang, J.Y. Wu, Organometallics 23 (2004) 3921.
[22] T.-Y. Dong, K. Chen, M.C. Lin, L. Lee, Organometallics 24 (2005) 4198.
[23] T.-Y. Dong, C.H. Huang, C.K. Chang, Y.S. Wen, S.L. Lee, J.A. Chen, W.Y. Yeh, A. Yeh, J. Am. Chem. Soc. 115 (1993) 6357.
[24] T.-Y. Dong, S.W. Chang, S.F. Lin, M.C. Lin, Y.S. Wen, L. Lee, Organometallics 25 (2006) 2018.
[25] B.P. Sullivan, J.M. Calvert, T. Meyer, Inorg. Chem. 19 (1980) 1404.
[26] (a) H. Atzkern, B. Huber, F.H. Köhler, G. Müller, R. Müller, Organometallics 10 (1991) 238;
(b) E.E. Bunel, P. Campos, P. Ruz, L. Valle, I. Chadwick, M.S. Ana, G. Gonzalez, J.M. Manriquez, Organometallics 7 (1988) 474;
(c) D.O. Cowan, P. Shu, F.L. Hedberg, M. Rossi, T.J. Kistenmacher, J. Am. Chem. Soc. 101 (1979) 1304;
(d) R. Moulton, T.W. Weidman, K.P.C. Vollhardt, A.J. Bard, Inorg. Chem. 25 (1986) 1846;
(e) D. Obendorf, H. Schottenberger, C. Rieker, Organometallics 10 (1991) 1293.
[27] (a) J.E. Sutton, H. Taube, Inorg. Chem. 20 (1981) 3125;
(b) S. Ernst, V. Kasack, W. Kaim, Inorg. Chem. 27 (1988) 1146;
(c) F. Salaymeh, S. Berhane, R. Yusof, R. de la Rosa, E.Y. Fung, R. Matamoros, K.W. Lau, K.Q. Zheng, E.M. Kober, J.C. Curtis, Inorg. Chem. 32 (1993) 3895.
[28] M.M. Bhadbhade, A. Das, J.C. Jeffery, J.A. McCleverty, J.A. Navas Badiola, M.D. Ward, J. Chem. Soc., Dalton Trans. (1995) 2769.
[29] Y.S. Sohn, D.N. Hendrickson, H.B. Gray, J. Am. Chem. Soc. 93 (1971) 3603.
[30] R.E. Bazak, Adv. Photochem. 8 (1971) 227.
[31] K. Hutchison, J.C. Morris, T.A. Nile, J.L. Walsh, D.W. Thompson, J.D. Petersen, J.R. Schoonover, Inorg. Chem. 38 (1999) 2516.
[32] J.N. Braddock, T.J. Meyer, J. Am. Chem. Soc. 95 (1973) 3158.
[33] E.M. Kober, T.J. Meyer, Inorg. Chem. 21 (1982) 3967.
[34] B.J. Coe, D.W. Thompson, C.T. Culbertson, J.R. Schoonover, T.J. Meyer, Inorg. Chem. 34 (1995) 3385.
[35] U. Siemeling, J.V. der Brüggen, U. Vorfeld, B. Neumann, A. Stammler, H.-G. Stammler, A. Brockhinke, R. Plessow, P. Zanello, F. Laschi, F.F. de Biani, M. Fontani, S. Steenken, M. Stapper, G. Gurzadyan, Chem. Eur. J. 9 (2003) 2819.
[36] A.C. Benniston, V. Goulle, A. Harriman, J.-M. Lehn, B. Marczinke, J. Phys. Chem. 98 (1994) 7798.